Supplementary Information for **“Trapping and amplification of unguided mode EMIC waves in the radiation belt”**

Contents of this File

Supplementary Discussion

Reliability of Linear Theory for Explaining Observations

Blum et al. [1] developed the two-parameter proxy of EMIC growth based on linear theory [2], and found an association between EMIC growth and relativistic electron loss during storms. The linear growth proxy can well predict the statistical wave enhancement regions [3] as well as the specific wave events [4]. However, Saikin et al. [5] found that the calculated wave amplitudes are too low compared to the observation. As far as our information goes, the following reasons may be responsible for the mismatches between calculations and observations: nonlinear effects [6]; simplifications in calculating linear growth rates, e.g., the bi-Maxwellian distribution, the assumed ion abundance ratios and the neglecting of the hot ions of a few hundred keV [5]; the ambiguity of wave propagation and convective growth [7, 8]; the marginally stable assumption [9, 10].

Nonlinear effects tend to suppress wave amplitude for the intense waves [6], thus could not account for the underestimation of wave growth. In the present calculations, the ion distributions are based on observations, the assumed ion abundance ratios are derived from observed crossover frequency and cutoff frequency, and the hot ions of a few hundred keV are considered, therefore, all the parameters in the linear growth rate are more realistic.

For the guided mode, the wave behaviors near bi-ion frequency are complex, and the proportions of energies that experience absorption, transmission, or reflection are highly dependent on the ion abundance ratios [11–14]. Therefore, the ambiguity of ion abundance ratios may lead to the improper estimation of the integrated wave gain. In addition, the present study indicates that the spatial variation of ion abundance ratios may also influence the propagation of guided waves near the bi-ion frequency, which may be a candidate, besides the oblique excitation by heavy ions [15], to explain the origin of previously reported oblique linear or right-hand EMIC waves in the inner plasmasphere [16–18] or away from general peak occurrence regions [19]. Unlike the guided mode, the convective growth for the unguided mode is relatively simple, because the refractive index is approximately independent of the wave normal angle, which allows us to predict the wave behavior solely based on the global plasma conditions. Furthermore, as the wave vectors are approximately parallel to the magnetic field for the rays with parallel group velocity, Landau damping should not be prominent [20] (Landau damping rate should be zero for parallel $\mathbf{k}$ [21]);

and as the wavenumbers are small near cutoff frequency, cyclotron damping by heavy ions should also be insignificant [11].

Yue et al. [10] demonstrated an upper limit of growth rate for EMIC waves based on the observed ion distributions, indicating the importance of local growth, i.e., the disturbance intensity of the wave source may be dependent on the time integration. This scenario of the local growth of wave source makes the trapping and convective growth 'unnecessary', for the explanation of the observed wave intensity. The problem that either the local growth or the convective growth determines the observed wave amplitude in the source region can not be exactly solved based on the present observations, however, we can still do some exploration. According to X. Yu and Yuan [22], it typically needs a period of tens of minutes for a wave source to reach the saturation state without injection of free energy. Considering the western drift of hot ions with a speed of several km/s (for 10 keV), for the typical EMIC event with a scale size of $\sim 0.5L$ [23], the time scale of the refresh of anisotropy should be comparable with that of the saturation. In the present event recorded by Probe A on 15 December 2015, considering that the drift speed of 200 keV protons at $L = 3.2$ is approximately 30 km/s, and the calculated growth rates are relatively small, the observed hot proton distributions are more likely to be in the 'fresh' state. From Figure 3, the values of the calculated convective growth rates are in the same order of magnitude in the selected time-frequency region, does not match exactly the variation of the observed wave intensity, further indicating that the anisotropy is not significantly relaxed within the source region (otherwise the calculated growth rate should be relatively smaller in the region of intense waves) [9, 22]. Furthermore, the growth rates of the guided mode waves (please see Supplementary Figure S3) are in the same order of magnitude as that of the unguided mode waves (Figure 3). As the guided mode waves should experience imperfect reflection and wave vector obliquity, which may substantially reduce the repeated convective amplification [14, 24, 25], if the actual generation process of the observed unguided mode waves is also not significantly influenced by the reflection and convective amplification, the guided mode waves are supposed to be observed with the same intensity of the unguided mode waves. Considering that only the unguided mode waves are observed, and that the intense waves are just located within the predicted trapping region, the process of trapping and convective amplification may be important to facilitate the wave generation.

Spatial Inhomogeneity of Ion Abundance Ratios

The spatial distributions of the ion abundance ratios η_s in the inner magnetosphere have considerable uncertainty. The statistics using Dynamics Explorer-1 (DE-1) showed that the $\eta_{\mathrm{He}+}/\eta_{\mathrm{H}+}$ ratio decreases with L below $L \sim 2$ but increases with L over $L \sim 2 - 5$ [26]. The magnetoseismology study by Takahashi et al. [27] revealed that the average ion mass during the quiet period is $\sim 2.0 - 3.0$ outside the plasmasphere (identified by n_e larger than 100 cm^{-3}) but is lower than 2.0 inside the plasmasphere. Therefore, there is a general trend that the proton abundance increases from outside the plasmasphere to just inside the plasmasphere. In the event recorded by Probe A on 15 December 2015, the value of $\eta_{\mathrm{H}+}$ decreases from 92% at just outside the plasmapause (n_e is approximately 100 cm^{-3}) to 83% at higher L (n_e is approximately 30 cm^{-3}), as shown in Figure 2. In the event recorded by Probe A on 30 November 2015, the value of $\eta_{\mathrm{H}+}$ decreases from 92% at $L \sim 3.9$ (n_e is approximately 40 cm^{-3}) to 85% at higher L (n_e is approximately 20 cm^{-3}), as shown in Supplementary Figure 4 and Supplementary Figure 5. The value of $\eta_{\mathrm{H}+}$ increases with n_e in these results, consistent with the trends from previous studies. Moreover, the model-estimated values of $\eta_{\mathrm{He}+}/\eta_{\mathrm{H}+}$ according to Huba et al. [28] are approximately 5

Modification of Dispersion Relations by Hot Plasma

In the present study, the wave behaviors are investigated under cold plasma dispersion relations. Some recent studies have illustrated that the hot plasma effect can modify the dispersion relation by changing the value of wave number [29, 30] or vanishing the stopband [31] when hot protons with tens of keV share more than a few percent of the total number density. In the wave event recorded by Probe A on 15 December 2015, the partial density of hot protons with an energy exceeding 1 keV is approximately 0.5 cm^{-3} within $L \sim 2.9 - 5$ (not shown here), while the plasma density decreases from $\sim$ 100cm^{-3} at $L \sim 2.9$ to below 10 cm^{-3} beyond $L \sim 4.5$; i.e., the ratio of hot protons increases from $\sim$ 0.5% at just outside the plasmapause to higher than $\sim$ 5% beyond $L \sim 4.5$. Therefore, the hot plasma effect can be neglected for the observed inner waves, but may influence the convective growth process or propagation behavior for any potential electromagnetic perturbations near the cold plasma cutoff frequencies in the outer L-shell.

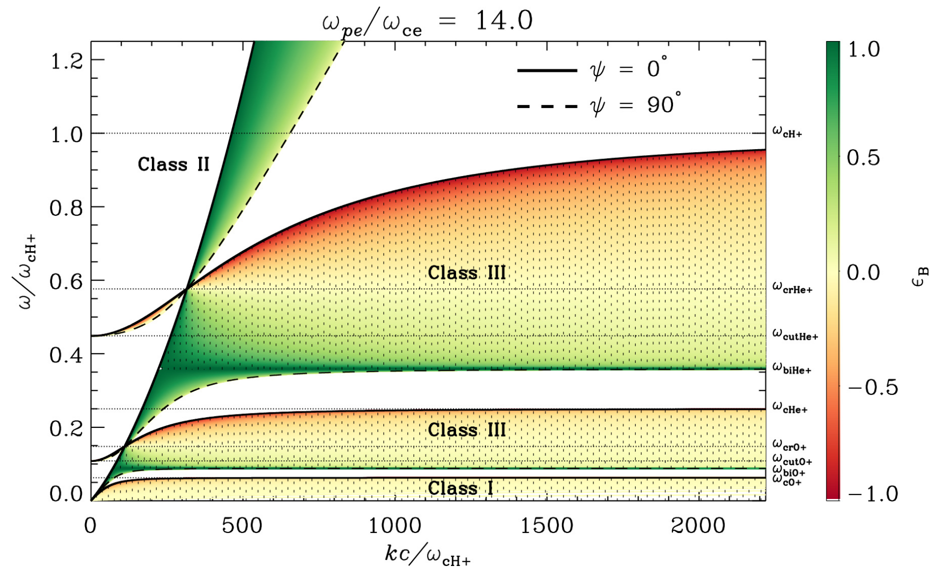

Supplementary Figure 1. Demonstration of the distribution of the ellipticity ϵ_B in ω-k space for wave modes near the H^+ gyrofrequency with different wave normal angles ψ. The magnitude of ϵ_B represents the ratio of the minor axis to the major axis of the magnetic field polarization ellipse in the plane perpendicular to the wave vector. A negative value represents left-hand rotation with respect to the ambient magnetic field, while a positive value represents right-hand rotation. The dispersion surfaces for the modes with parallel and perpendicular ψ are plotted as black solid and dashed curves, respectively. The guided modes are in the shaded areas, while the unguided modes are in the unshaded areas. The gyrofrequencies, crossover frequencies, bi-ion frequencies and cutoff frequencies are marked on the right side of the figure. Here, the magnitude of the background magnetic field is set to 400 nT, and the electron number density is 300 cm^{-3}; thus, the $\omega_{\rm pe}/\omega_{\rm ce}$ ratio is approximately 14. The ion abundance ratios are set to 70% H^+, 20% He^+ and 10% O^+.

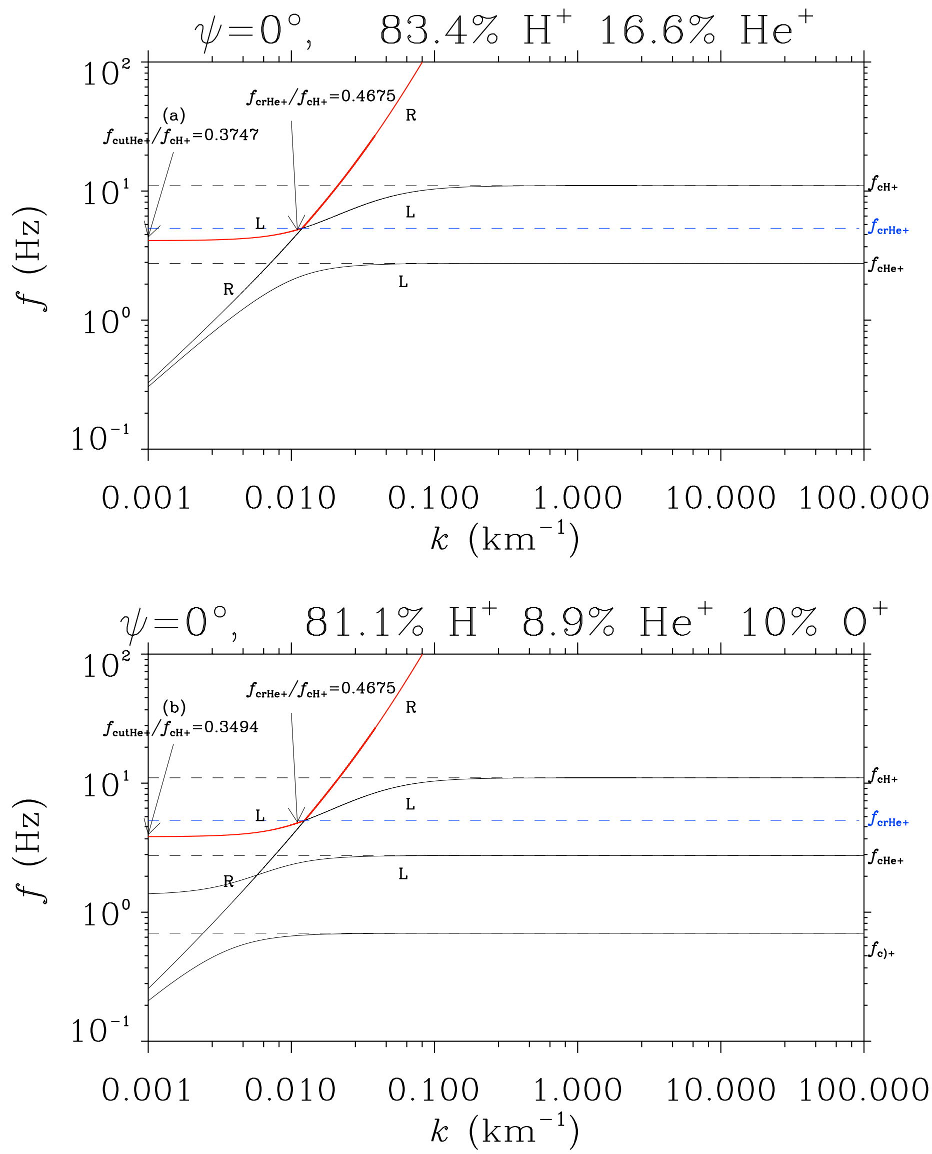

Supplementary Figure 2. Dispersion curves around gyrofrequencies of ions. (a) The plasma contains no O^+ ions. (b) The plasma contains 10% O^+ ions. For each case, the ratio of He^+ crossover frequency to H^+ gyrofrequency f_{crHe+}/f_{cH+} is set to 0.4675, and the abundance ratios of H^+ and He^+ are obtained accordingly. One can find that the differences of the dispersion curves for each mode in H^+ band are small.

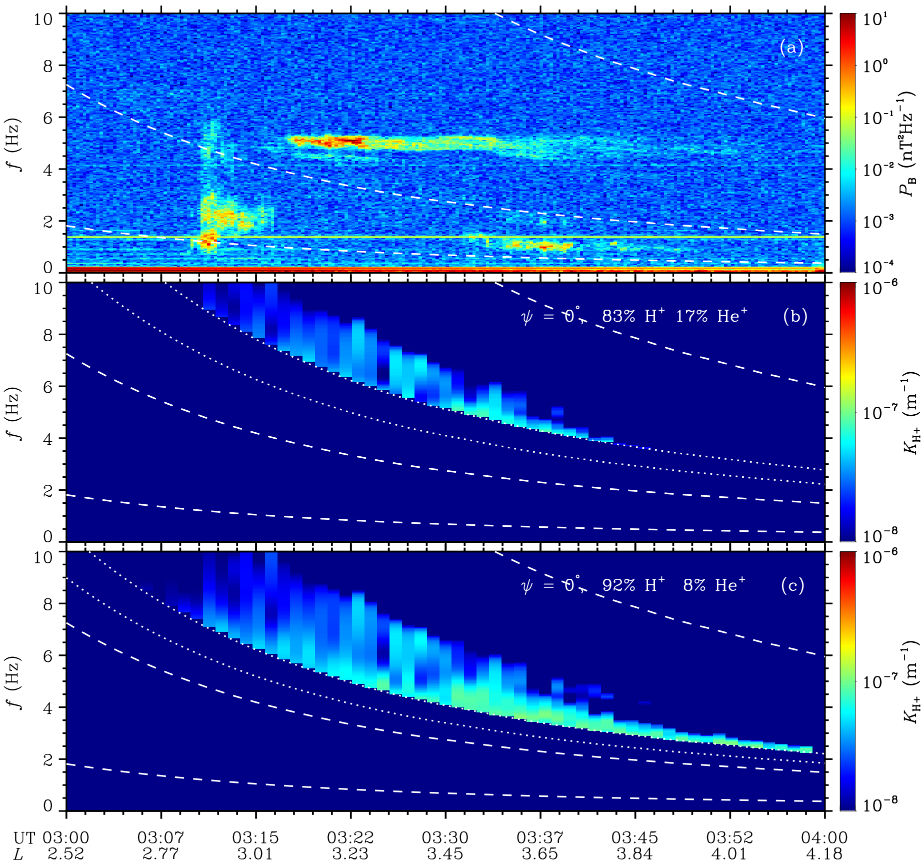

Supplementary Figure 3. Wave growth analysis for the guided mode, in the event recorded by Probe A on 15 December 2015: (a) The observed magnetic power spectral density P_B; (b,c) Wave convective growth rates $K_{\mathrm{H+}}$ contributed by H^+. The dashed curves mark the gurofrequencies, while the dotted curves mark the He^+ crossover frequency $f_{\mathrm{crHe+}}$ and He^+ cutoff frequency $f_{\mathrm{cutHe+}}$.

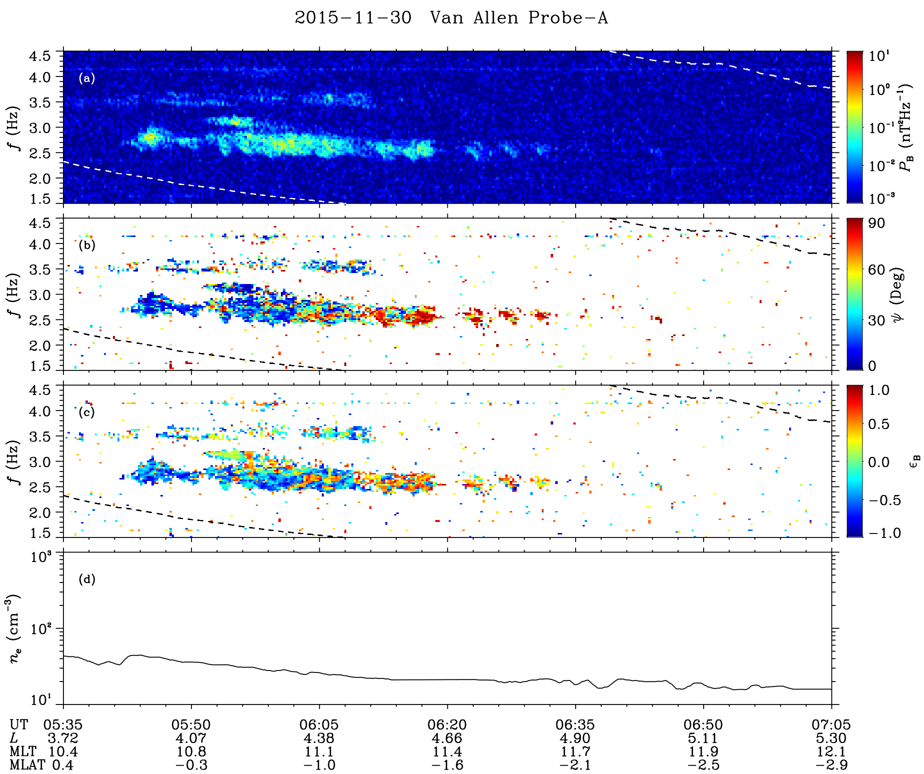

Supplementary Figure 4. Wave properties of the event recorded by Probe A on 30 November 2015: (a) magnetic power spectral density P_B, (b) normal angle ψ (unifying the two field-aligned orientations), (c) ellipticity ϵ_B. (d) The background electron number density n_e.

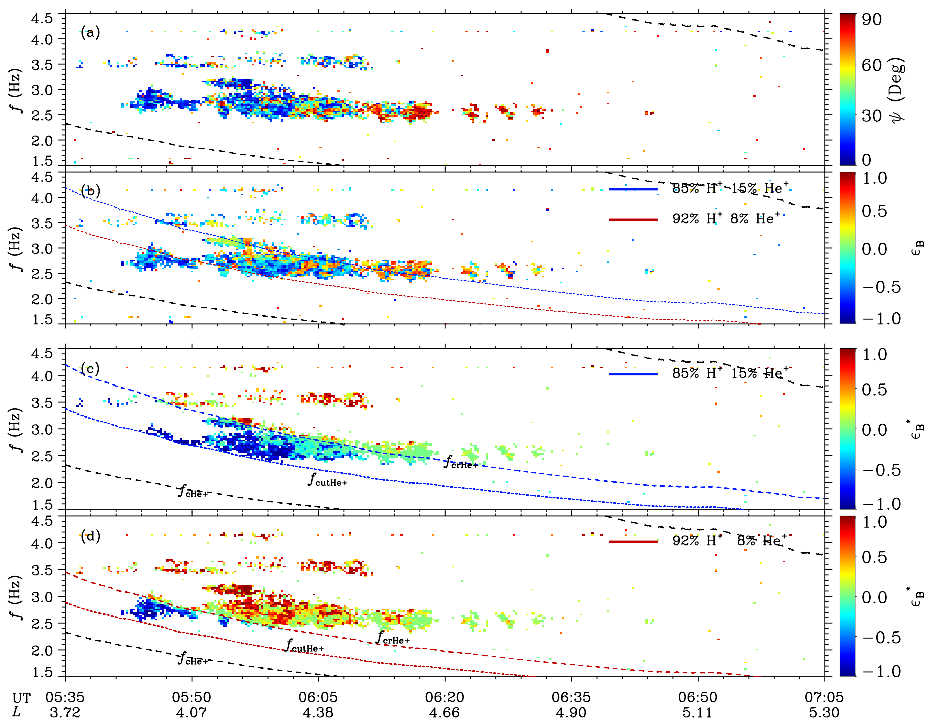

Supplementary Figure 5. Verification of the crossover frequency and estimation of the ion abundance ratios for the event recorded by Probe A on 30 November 2015. (a,b) The observed wave normal angle ψ and ellipticity ϵ_B. The colored curves trace the He^+ crossover frequency $f_{\mathrm{crHe+}}$ for different ion abundance ratios. (c,d) The theoretically calculated distribution of the ellipticity ϵ_B^* for the given constant ion abundance ratios.

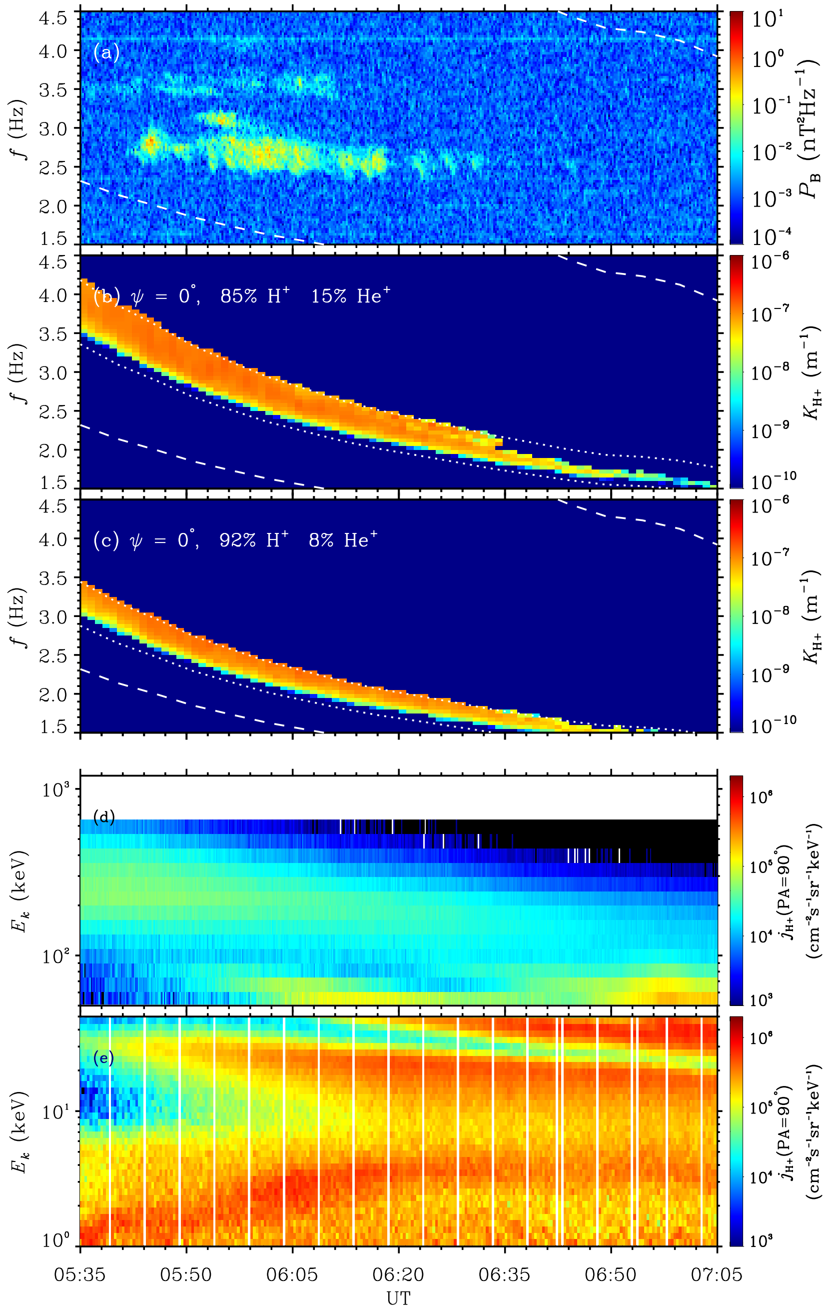

Supplementary Figure 6. Wave growth analysis for the unguided mode, in the event recorded by Probe A on 30 November 2015: (a) The observed magnetic power spectral density P_B; (b,c) Wave convective growth rates $K_{\mathrm{H+}}$ contributed by H^+; and Energy-dependent H^+ differential fluxes $j_{\mathrm{H+}}$ at a 90° pitch angle measured by (d) RBSPICE and (e) HOPE.

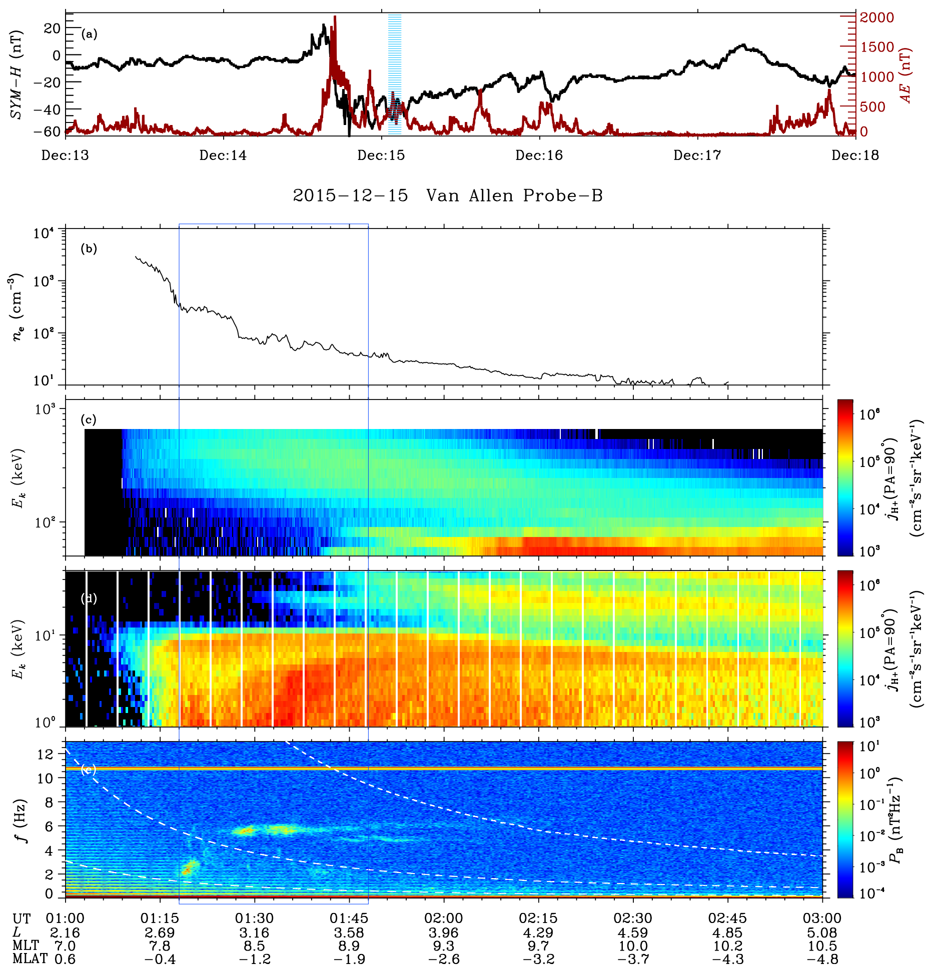

Supplementary Figure 7. Overview of the unguided mode wave event recorded by Probe B on 15 December 2015: (a) SYM-H index and AE index (shaded region marks the period of the wave event); (b) background electron number density n_e (dashed lines for the location of the plasmapause); (c,d) energy-dependent H^+ differential fluxes j_{H+} at a 90° pitch angle; and (e) magnetic power spectral density P_B (white dashed curves trace the local gyrofrequencies of hydrogen, helium, and oxygen from top to bottom).

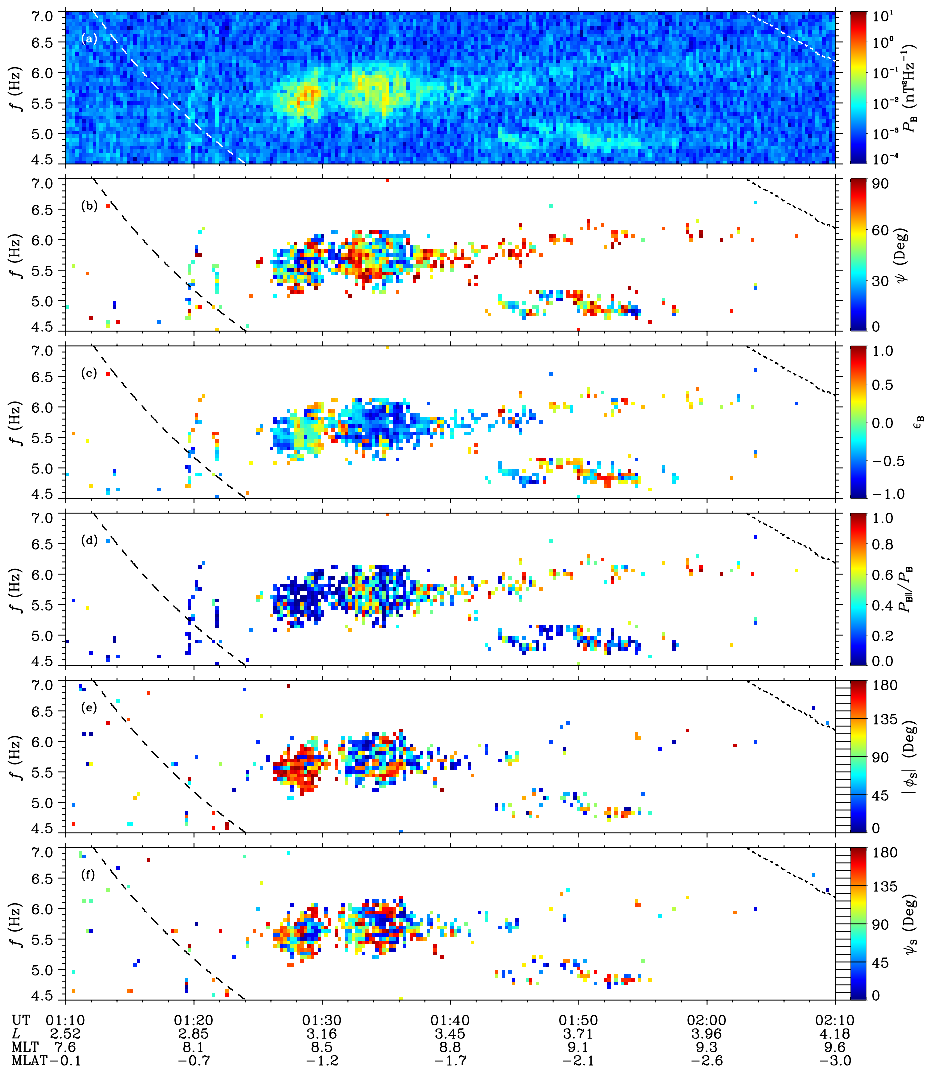

Supplementary Figure 8. Wave properties of the event recorded by Probe B on 15 December 2015: (a) magnetic power spectral density P_B, (b) wave normal angle ψ (unifying the two field-aligned orientations), (c) ellipticity ϵ_B, (d) magnetic compression ratio $P_{B\|}/P_B$, (e) azimuthal angle of the Poynting flux ϕ_S (0° represents away from the Earth), and (f) angle of the Poynting flux with respect to the ambient magnetic field ψ_S.

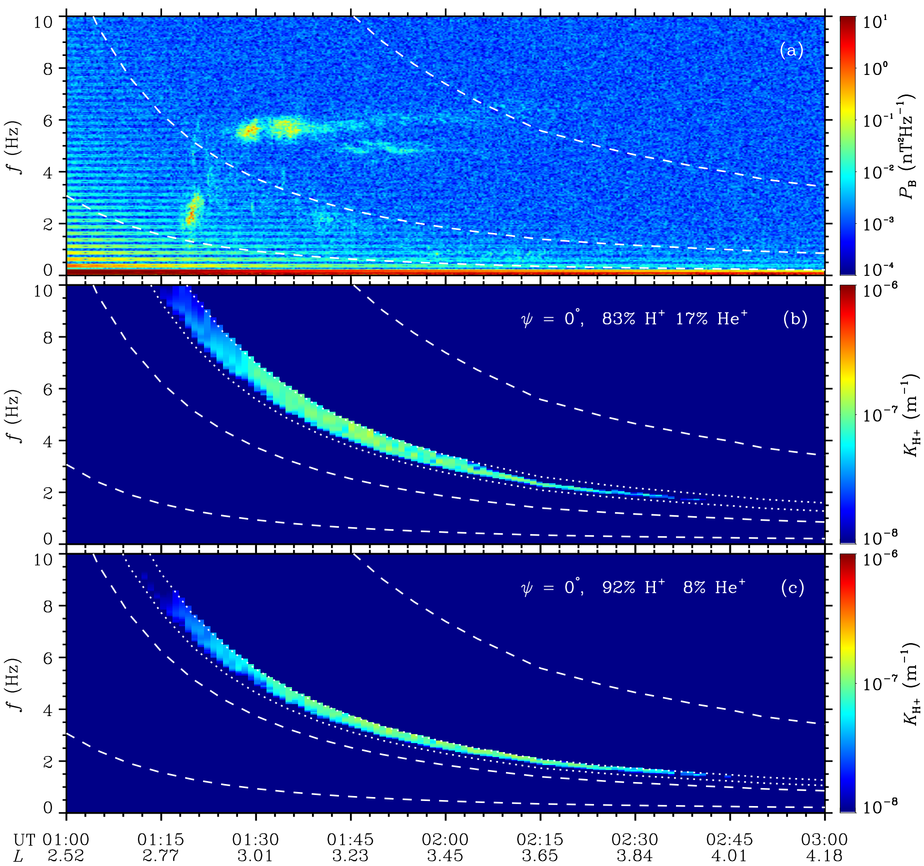

Supplementary Figure 9. Wave growth analysis for the unguided mode, in the event recorded by Probe B on 15 December 2015. The illustrations are the same as those in Figure 3.

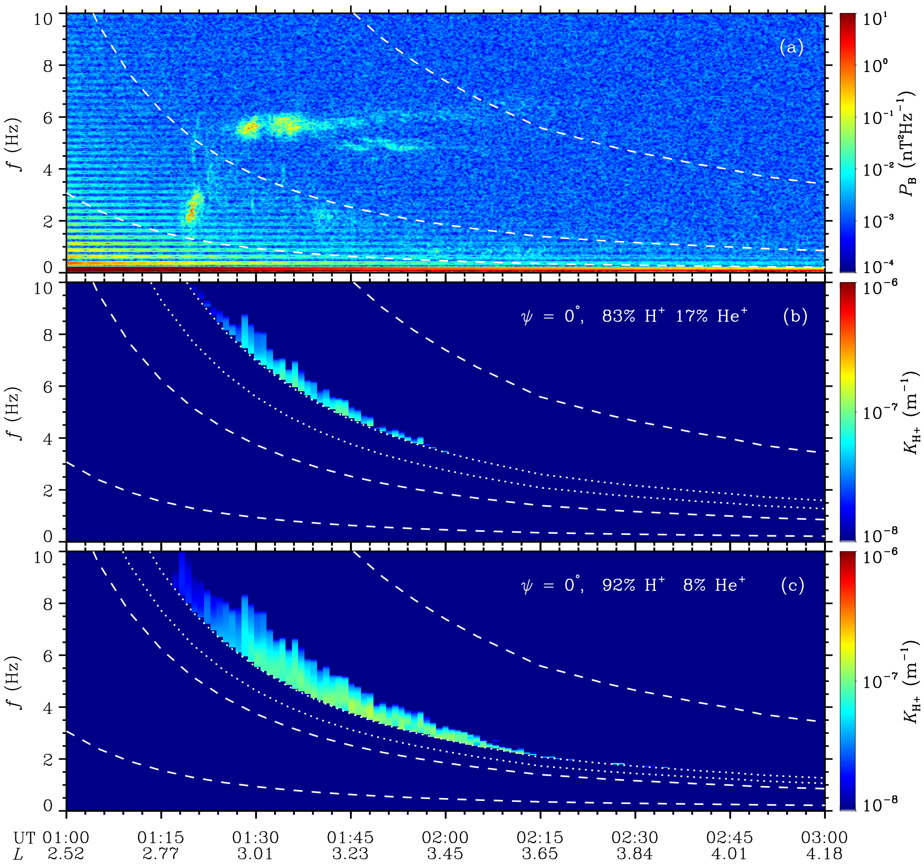

Supplementary Figure 10. Wave growth analysis for the guided mode, in the event recorded by Probe B on 15 December 2015. The illustrations are the same as those in Figure 3.

Supplementary References

[1] Lauren W. Blum et al. "Ion observations from geosynchronous orbit as a proxy for ion cyclotron wave growth during storm times". In: *J. Geophys. Res. (Space Physics)* 114.A10, A10214 (Oct. 2009), A10214. DOI: 10.1029/2009JA014396.

[2] S. Peter Gary. *Theory of Space Plasma Microinstabilities.* 1993.

[3] R. C. Allen et al. "A statistical study of EMIC waves observed by Cluster: 2. Associated plasma conditions". In: *J. Geophys. Res. (Space Physics)* 121.7 (July 2016), pp. 6458–6479. DOI: 10.1002/2016JA022541.

[4] J.-C. Zhang et al. "Excitation of EMIC waves detected by the Van Allen Probes on 28 April 2013". In: *Geophys. Res. Lett.* 41 (June 2014), pp. 4101–4108. DOI: 10.1002/2014GL060621.

[5] A. A. Saikin et al. "Comparing simulated and observed EMIC wave amplitudes using in situ Van Allen Probes' measurements". In: *J. Atmos Sol.-Terr. Phy.* 177 (Oct. 2018), pp. 190–201. DOI: 10.1016/j.jastp.2018.01.024.

[6] Y. Omura et al. "Theory and observation of electromagnetic ion cyclotron triggered emissions in the magnetosphere". In: *J. Geophys. Res. (Space Physics)* 115, A07234 (July 2010), A07234. DOI: 10.1029/2010JA015300.

[7] R. M. Thorne and R. B. Horne. "Comment on Khazanov et al. [2002] and Khazanov et al. [2006]". In: *J. Geophys. Res. (Space Physics)* 112.A12, A12214 (Dec. 2007), A12214. DOI: 10.1029/2007JA012268.

[8] G. V. Khazanov et al. "Reply to comment by R. M. Thorne and R. B. Horne on Khazanov et al. [2002] and Khazanov et al. [2006]". In: *J. Geophys. Res. (Space Physics)* 112.A12, A12215 (Dec. 2007), A12215. DOI: 10.1029/2007JA012463.

[9] S. Peter Gary and Martin A. Lee. "The ion cyclotron anisotropy instability and the inverse correlation between proton anisotropy and proton beta". In: *J. Geophys. Res.* 99.A6 (June 1994), pp. 11297–11302. DOI: 10.1029/94JA00253.

[10] Chao Yue et al. "The Relationship Between EMIC Wave Properties and Proton Distributions Based on Van Allen Probes Observations". In: *Geophys. Res. Lett.* 46.8 (Apr. 2019), pp. 4070–4078. DOI: 10.1029/2019GL082633.

[11] R. M. Thorne and R. B. Horne. "Cyclotron absorption of ion-cyclotron waves at the bi-ion frequency". In: *Geophys. Res. Lett.* 20 (Feb. 1993), pp. 317–320. DOI: 10.1029/93GL00089.

[12] R. B Horne and R. M Throne. "Wave heating of He + by electromagnetic ion cyclotron waves in the magnetosphere' Heating near the H+-He + bi-ion resonance frequency". In: *J. Geophys. Res.* 102 (1997), pp. 11,457–11,471. DOI: 10.1029/97JA00749.

[13] G. V. Khazanov et al. “Self-consistent model of magnetospheric ring current and propagating electromagnetic ion cyclotron waves: Waves in multi-ion magnetosphere”. In: *J. Geophys. Res. (Space Physics)* 111.A10, A10202 (Oct. 2006), A10202. DOI: 10.1029/2006JA011833.

[14] Y. Hu, R. E. Denton, and J. R. Johnson. “Two-dimensional hybrid code simulation of electromagnetic ion cyclotron waves of multi-ion plasmas in a dipole magnetic field”. In: *J. Geophys. Res.* 115, A09218 (Sept. 2010), p. 9218. DOI: 10.1029/2009JA015158.

[15] Konstantin V. Gamayunov et al. “Generation of EMIC Waves Observed by Van Allen Probes at Low L Shells”. In: *J. Geophys. Res. (Space Physics)* 123.10 (Oct. 2018), pp. 8533–8556. DOI: 10.1029/2018JA025629.

[16] A. A. Saikin et al. “The occurrence and wave properties of H^+-, He^+-, and O^+-band EMIC waves observed by the Van Allen Probes”. In: *J. Geophys. Res. (Space Physics)* 120 (Sept. 2015), pp. 7477–7492. DOI: 10.1002/2015JA021358.

[17] B. Grison et al. “Cluster observations of reflected EMIC-triggered emission”. In: *Geophys. Res. Lett.* 43 (May 2016), pp. 4164–4171. DOI: 10.1002/2016GL069096.

[18] G. Wang et al. “Propagation of EMIC Waves Inside the Plasmasphere: A Two-Event Study”. In: *J. Geophys. Res. (Space Physics)* 124.11 (Nov. 2019), pp. 8396–8415. DOI: 10.1029/2019JA027055.

[19] X. Y. Wang et al. “The occurrence and wave properties of EMIC waves observed by the Magnetospheric Multiscale (MMS) mission”. In: *J. Geophys. Res. (Space Physics)* 122.8 (Aug. 2017), pp. 8228–8240. DOI: 10.1002/2017JA024237.

[20] R. M. Thorne and R. B. Horne. “The contribution of ion-cyclotron waves to electron heating and SAR-arc excitation near the storm-time plasmapause”. In: *Geophys. Res. Lett.* 19 (Feb. 1992), pp. 417–420. DOI: 10.1029/92GL00089.

[21] C. Kennel. “Low-Frequency Whistler Mode”. In: *Phys. Fluids* 9 (Nov. 1966), pp. 2190–2202. DOI: 10.1063/1.1761588.

[22] Xiongdong Yu and Zhigang Yuan. “Saturation Characteristics of Parallel EMIC Waves in the Inner Magnetosphere”. In: *Geophys. Res. Lett.* 46.14 (July 2019), pp. 7902–7910. DOI: 10.1029/2019GL083630.

[23] L. W. Blum et al. “EMIC wave scale size in the inner magnetosphere: Observations from the dual Van Allen Probes”. In: *Geophys. Res. Lett.* 44 (Feb. 2017), pp. 1227–1233. DOI: 10.1002/2016GL072316.

[24] R. B. Horne and R. M. Thorne. “On the preferred source location for the convective amplification of ion cyclotron waves”. In: *J. Geophys. Res.* 98 (June 1993), pp. 9233–9247. DOI: 10.1029/92JA02972.

[25] T. M. Loto’Aniu, B. J. Fraser, and C. L. Waters. “Propagation of electromagnetic ion cyclotron wave energy in the magnetosphere”. In: *J. Geophys. Res.* 110, A07214 (July 2005), A07214. DOI: 10.1029/2004JA010816.

[26] J. Goldstein et al. “Temperature Dependence of Plasmaspheric Ion Composition”. In: *J. Geophys. Res. (Space Physics)* 124.8 (Aug. 2019), pp. 6585–6595. DOI: 10.1029/2019JA026822.

[27] K. Takahashi et al. “Mass density inferred from toroidal wave frequencies and its comparison to electron density”. In: *J. Geophys. Res. (Space Physics)* 111, A01201 (Jan. 2006), A01201. DOI: 10.1029/2005JA011286.

[28] J. Huba and J. Krall. “Modeling the plasmasphere with SAMI3”. In: *Geophys. Res. Lett.* 40.1 (Jan. 2013), pp. 6–10. DOI: 10.1029/2012GL054300.

[29] Xing Cao et al. “Scattering of Ultra-relativistic Electrons in the Van Allen Radiation Belts Accounting for Hot Plasma Effects”. In: *Sci. Rep.* 7, 17719 (2017), p. 17719. DOI: 10.1038/s41598-017-17739-7.

[30] Binbin Ni et al. “Hot Plasma Effects on the Cyclotron-Resonant Pitch-Angle Scattering Rates of Radiation Belt Electrons Due to EMIC Waves”. In: *Geophys. Res. Lett.* 45.1 (2018), pp. 21–30. DOI: 10.1002/2017GL076028.

[31] L. Chen, R. M. Thorne, and J. Bortnik. “The controlling effect of ion temperature on EMIC wave excitation and scattering”. In: *Geophys. Res. Lett.* 38, L16109 (Aug. 2011), p. L16109. DOI: 10.1029/2011GL048653.